INTERNATIONAL JOURNAL FOR NUMERICAL AND ANALYTICAL METHODS IN GEOMECHANICS, VOL. 20, 815–830 (1996)

THEORETICAL ANALYSIS OF AN IMPERVIOUS, HEATED-CYLINDER 'GROUNDWATER VELOCIMETER'

JOSEPH R. FELDKAMP

Applied Research Associates, Inc., Building 1117, 139 Barnes Drive, Tyndall AFB, FL 32403, U.S.A.

SUMMARY

An isothermally heated, impervious cylinder, which is placed normal to the path of flowing groundwater, is theoretically evaluated for its potential to serve as a kind of 'groundwater velocimeter'. The essential task is to determine whether the *variation* in heat output along the cylinder perimeter is sufficiently large to permit measurement for typical groundwater velocities. Using finite elements, the governing equations of advective thermal transport in saturated porous media are solved to obtain the variation in heat output along the circumference of the heated cylinder. An annular region of different hydraulic conductivity is assumed to separate the cylinder from the surrounding formation. The creation of such a region during placement of a cylinder is inevitable. A parametric study led to the following conclusions: (1) A smaller cylinder radius is preferable since the time to achieve a particular degree of asymmetry in heat output is then greatly reduced. (2) An annular region of lower hydraulic conductivity, relative to formation, reduces output asymmetry by no more than 25%, but if hydraulic conductivity is increased, output asymmetry can increase several times. (3) For annular regions having a higher hydraulic conductivity than the surrounding formation, annular thickness is not important. (4) The least groundwater speed which may be accurately measured by such a device will depend heavily upon instrumentation but is tentatively placed at about $5{\cdot}0 \times 10^{-5}$ cm/s. Theoretical results are approximately confirmed by preliminary experiments with a prototype device which has been constructed so as to *directly* measure the expected variation in thermal output. Partial construction details are provided.

KEY WORDS: groundwater; velocity; heat transquent; heated cylinder

INTRODUCTION

Assuming a *static* liquid phase, thermal output along the periphery of an impervious, isothermally heated cylinder embedded in a saturated porous medium is expected to be invariant with respect to angular location. The isotherms, or contours of constant temperature, would form a family of circles, all concentric with the axis of the heated cylinder. The time-dependent solution for this particular problem was published some time ago by Jaeger[1].

In the event that the isothermally heated cylinder is placed perpendicular to a uniform groundwater flow field, the previously concentric isotherms are expected to be displaced downstream and the thermal flux from cylinder surface to porous medium is expected to vary along the cylinder's perimeter as well as with time. It is this asymmetry in thermal output from the cylinder that will be the focus of this paper. The motivation for considering such a problem is an interest in testing whether or not the variation in thermal output is sufficiently substantial that it could be measured by some means. If thermal output asymmetry is measurable for reasonable groundwater velocities, then the feasibility of measuring groundwater velocity through such a device would have been demonstrated.

CCC 0363–9061/96/110815–16
© 1996 by John Wiley & Sons, Ltd.
Received 11 December 1995
Revised 8 March 1996

Efforts have already been made in previous work by Melville *et al.*[2] to determine whether or not the measurement of *temperature* asymmetry along the surface of a *pervious*, heated cylinder could be interpreted to yield a measurement of groundwater velocity. Inside such a device, a centrally located heat source discharges heat into the porous cylinder and ultimately into the surrounding formation. An attempt to simulate the degree of temperature asymmetry on the cylinder surface by computer would require an analysis of heat flow both inside and outside the cylindrical zone. Because of additional complications associated with hydraulic conductivity contrasts between cylinder and formation, the calibration of device response has been attempted through empirical means. A similar device has been described in the patent literature by Dunn *et al.*[3] which places heat sources as well as temperature sensors on the cylinder surface.

For the problem of interest to this paper, an analysis of heat flow and mass transfer is necessary only for the region external to the isothermally heated cylinder. This follows since the cylinder is hydraulically impervious *and* has a known surface temperature. Both features serve as key boundary conditions. To increase the realism of analysis, an annular zone having a different hydraulic conductivity than the surrounding geologic formation is presumed to separate the cylinder and the formation. This feature was not included in the analysis given by van der Star *et al.*[4] where the finite difference method was used to process the governing equations. If such a heated cylinder were installed for the purpose of groundwater velocity measurement, the appearance of an annular region of different hydraulic conductivity would be inevitable. As we shall see, the consequences are enormous.

Subsequent to a theoretical and finite element analysis of heat flow in the heterogeneous porous medium that surrounds the isothermally heated cylinder, a brief presentation is given of experience acquired with a prototype device that measures the variation in thermal output along the perimeter of the heated cylindrical surface. Partial construction details will be provided plus some preliminary data acquired with the device in a laboratory sandbox approximately 1·5 m and 0·5 m deep.

THEORETICAL BACKROUND

With reference to Figure 1, the impervious cylinder, heated to temperature T_a and having radius 'a', is surrounded by an annular material with hydraulic conductivity K_a and thickness $b - a$. The

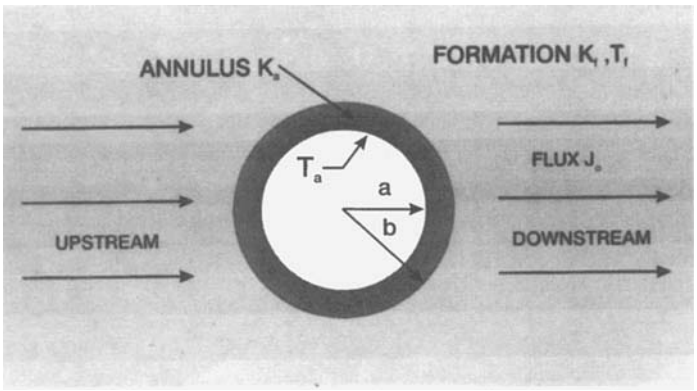

Figure 1. Sketch of the system, showing the heated cylinder oriented perpendicular to flowing groundwater and surrounded by an annular region of hydraulic conductivity $K_a \neq K_f$

formation material outside the annular zone has hydraulic conductivity K_f, and at large distances from the heated cylinder the formation temperature is given by its initial background value T_f. The uniform groundwater flow field passing through the formation *prior* to insertion of the cylinder and annulus is given in the figure by J_0. The return to a uniform flow field of flux J_0 at distances large compared to 'a' will in fact serve as an important boundary condition.

In order to reduce model complexity, certain simplifying approximations were made, similar to those made by van der Star *et al.*:[4] neglect of natural convection; neglect of mechanical dispersion effects; neglect of heat generation due to viscous dissipation; and finally neglect of temperature differences between pore fluid and contiguous soil particles. The neglect of natural convection is acceptable if vertical temperature gradients are negligible. In view of these assumptions, the expressions for heat flux, $\mathbf{q}$, and for conservaton of internal energy, U_b, are as follows:

$$\mathbf{q} = -k_s \nabla T + U_w \mathbf{J} \tag{1}$$

$$\nabla \cdot \mathbf{q} = -\frac{\partial U_b}{\partial t} \tag{2}$$

where T is temperature, k_s is thermal conductivity (power/unit area/unit T gradient), U_w is internal energy of pore fluid/unit volume of pore fluid, U_b is internal energy of bulk soil/unit volume of soil, $\mathbf{J}$ is volumetric flux of pore fluid (volume flow rate/unit area) and t is time.

Though the medium is considered heterogeneous with regard to hydraulic properties, it is considered homogeneous with regard to the soil thermal conductivity, k_s.

The appropriate expression for the flux $\mathbf{J}$ is obtained by solving Laplace's equation for the piezometric head in each of the two isotropic, homogeneous regions surrounding the impervious cylinder and then enforcing required boundary conditions at $r = a$, $r = b$ and $r \to \infty$. The solution procedure is considered routine, using so-called cylindrical harmonics in the separation-of-variables context as in Reitz and Milford.[5] The flux components, given in cylindrical co-ordinates, are:

inside annular zone:

$$j_r = J_0 \alpha \left(1 - \frac{a^2}{r^2}\right) \cos \vartheta \tag{3}$$

$$j_\vartheta = -J_0 \alpha \left(1 + \frac{a^2}{r^2}\right) \sin \vartheta \tag{4}$$

$$\alpha = \frac{2K_a b^2}{b^2(K_a + K_f) - a^2(K_a - K_f)} \tag{5}$$

outside annular zone:

$$j_r = J_0 \left(1 - \beta \frac{a^2}{r^2}\right) \cos \vartheta \tag{6}$$

$$j_\vartheta = -J_0 \left(1 + \beta \frac{a^2}{r^2}\right) \sin \vartheta \tag{7}$$

$$\beta = \frac{a^2 b^2 (K_a + K_f) - b^4 (K_a - K_f)}{a^2 b^2 (K_a + K_f) - a^4 (K_a - K_f)} \tag{8}$$

where 'r' and 'ϑ' are the customary cylindrical co-ordinates. Extreme downstream and upstream locations are obtained when $\vartheta = 0$ and $\vartheta = \pi$, respectively, while $\delta\vartheta > 0$ is taken as the counter-clockwise sense.

In order to formulate a partial differential equation (p.d.e.) from the above equations, heat capacities for both water and bulk soil must be introduced. In differential form,

$$dU_w = C_{pw}\,dT \tag{9}$$

$$dU_b = C_{pb}\,dT \tag{10}$$

where the heat capacities are at constant pressure and have units of energy per unit volume per unit temperature. The heat capacity of bulk soil, C_{pb}, was evaluated with the aid of a relation given by Bear:[6]

$$C_{pb} = nC_{pw} + (1 - n)C_{ps} \tag{11}$$

where 'n' is soil porosity and C_{ps} is the heat capacity of the solids within some representative elementary volume.

In order to achieve enhanced resolution of the temperature field in the vicinity of the heated cylinder, the radial axis was logarithmically transformed prior to finite element analysis. Such resolution is important since power flux, and therefore the component of the temperature gradient normal to the cylinder surface, is the desired quantity. The needed transformation is given by

$$\lambda = \ln(r/a) \tag{12}$$

The form of the governing p.d.e. resulting from appropriate combination of the foregoing equations is

$$\frac{\partial T}{\partial \tau} = e^{-2\lambda}\left[\frac{\partial^2 T}{\partial \lambda^2} + \frac{\partial^2 T}{\partial \vartheta^2}\right] - \varepsilon e^{-\lambda}\left[j_r'\frac{\partial T}{\partial \lambda} + j_\vartheta'\frac{\partial T}{\partial \vartheta}\right] \tag{13}$$

Dimensionless time τ is related to real time through

$$\tau = \frac{k_s t}{C_{pb}a^2} \tag{14}$$

while the dimensionless parameter ε is given by

$$\varepsilon = \frac{C_{pw}J_0 a}{k_s} \tag{15}$$

ε becomes a 'porous-medium' Peclet number, $\equiv Pe$, when 'a' is the characteristic grain size in the porous medium rather than the cylinder radius. Primes are attached to the hydraulic flux components as they are now rendered dimensionless due to a division by J_0. Since ε is of the order of unity (implying $Pe \ll 1$), a perturbative approach to solving (13) is not useful. Redefining the temperature in (13) to be a dimensionless temperature via the transformation

$$T \leftarrow \frac{T - T_f}{T_a - T_f} \tag{16}$$

leaves the form of (13) unchanged. Dimensionless temperature ranges from 1 at the cylinder surface to 0 infinitely far away.

FINITE ELEMENT ANALYSIS

The finite element method was used to solve equation (13), subject to appropriate boundary conditions. The domain of interest, $0 \leqslant \vartheta \leqslant \pi$ and $0 \leqslant \lambda \leqslant 2$, was subdivided into a 150-element rectangular mesh, with element and node labels as shown in Figure 2. Provided τ is sufficiently small, the value of 'r' corresponding to $\lambda = 2$ may be regarded, for all practical purposes, as infinitely far from the cylinder surface. The limitations imposed on τ will be discussed later. Boundary conditions are quite simple:

$$T = 1, \lambda = 0 \tag{17a}$$

$$T = 0, \lambda = 2 \text{ (corresponds with } r \cong 7.4a) \tag{17b}$$

$$\partial T/\partial \vartheta = 0, \vartheta = 0 \text{ and } \vartheta = \pi, \text{ for } \lambda\colon 0 \leqslant \lambda \leqslant 2 \tag{17c}$$

If desired, some spatial variation in T along the $\lambda = 0$ boundary may be accommodated but was not used in any calculations reported herein.

The dimensionless temperature T is expanded into a finite sum of two-dimensional piecewise linear basis functions, ϕ_j, with j referring to one of the 176 mesh nodes:

$$T = \sum_j T_j(\tau)\,\phi_j(\lambda, \vartheta) \tag{18}$$

Note that the time dependence is carried by the nodal temperature coefficients, T_j. Using the $\{\phi_i\}$ also as weight functions, but excluding those ϕ_i whose nodes i fall on the $\lambda = 0$ or $\lambda = 2$ boundaries, a weighted residual approach led to the following integral equations:

$$-\sum_j \dot{T}_j A_{ij} = \Lambda_i \tag{19a}$$

$$\Lambda_i = \sum_j T_j(B_{ij} + C_{ij} + \varepsilon D_{ij} + \varepsilon E_{ij}) \tag{19b}$$

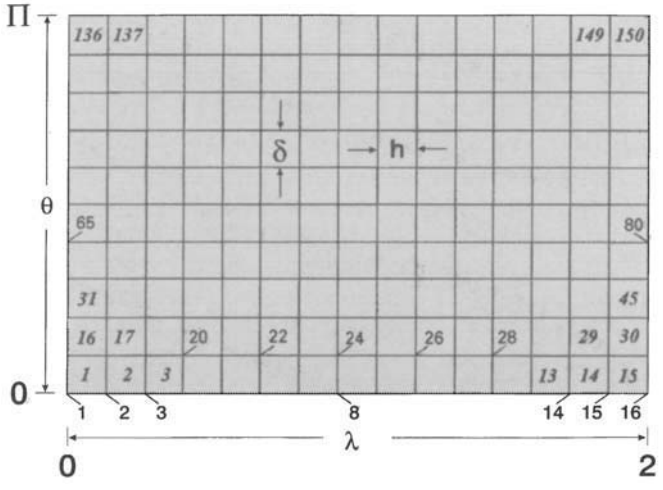

Figure 2. Finite element mesh in λ, θ space. Both nodal and element labels are partially provided

The dot just above T_j implies time differentiation while the matrix coefficients, $A_{ij} \ldots E_{ij}$, are given by sums of the elemental integrals:

$$A_{ij} = \sum_k \iint_{R_k} \phi_i \phi_j \, d\lambda \, d\vartheta \tag{20a}$$

$$B_{ij} = \sum_k \iint_{R_k} \frac{\partial}{\partial \lambda} (e^{-2\lambda} \phi_i) \frac{\partial \phi_j}{\partial \lambda} d\lambda \, d\vartheta \tag{20b}$$

$$C_{ij} = \sum_k \iint_{R_k} \frac{\partial}{\partial \vartheta} (e^{-2\lambda} \phi_i) \frac{\partial \phi_j}{\partial \vartheta} d\lambda \, d\vartheta \tag{20c}$$

$$D_{ij} = \sum_k \iint_{R_k} \phi_i e^{-\lambda} j_r \frac{\partial \phi_j}{\partial \lambda} d\lambda \, d\vartheta \tag{20d}$$

$$E_{ij} = \sum_k \iint_{R_k} \phi_i e^{-\lambda} j_\vartheta \frac{\partial \phi_j}{\partial \lambda} d\lambda \, d\vartheta \tag{20e}$$

In writing the integrals, (20a–20e), an integration by parts was used together with boundary conditions and the fact that all those ϕ_i which are used as weight functions vanish on the boundaries $\lambda = 0, 2$. The total number of degrees of freedom (d.o.f.) equals 154. Integrals D_{ij} and E_{ij} were obtained numerically through Gauss quadrature, while the others were obtained analytically.

Given the particular elemental and nodal labelling scheme shown in Figure 2, it proved advantageous to reorganize the vector of unknowns, $\{\dot{T}_j\}$, into a 14×11 matrix of unknowns. Column 1 contained those $\dot{T}_j$ with $j = 2, 3, \ldots, 15$; column 2 those $\dot{T}_j$ with $j = 18, 19, \ldots, 31$ and so on. The final column contains those $\dot{T}_j$ with $j = 162, 163, \ldots, 175$. Similarly, the vector Λ_i was organized into an 11×14 matrix. Row 1 contained those Λ_i with $i = 2, 3, \ldots, 15$; row 2 those Λ_i with $i = 18, 19, \ldots, 31$ and so on. The final row contains those Λ_i with $i = 162, 163, \ldots, 175$. The resulting set of reorganized equations takes on a very compact form:

$$\frac{h\delta}{36} \mathbf{B}(\mathbf{AT})^{\mathrm{T}} = \mathbf{F} \tag{21}$$

Boldface indicates matrix quantities, with $\mathbf{T}$ the matrix containing the $\dot{T}_j$ as described and the $\mathbf{F}$ matrix containing the Λ_i as described. The forms of the matrices $\mathbf{A}$ and $\mathbf{B}$ are particularly simple. $\mathbf{A}$ is a 14×14 tridiagonal matrix with all diagonal elements = 4 and all off-diagonal elements = 1. $\mathbf{B}$ is an 11×11 tridiagonal matrix with all diagonal elements = 4 except for first and last entries along the diagonal which are = 2. Off-diagonal elements in $\mathbf{B}$ are all = 1. The equations given by (21) represent a set of ordinary differential equations (o.d.e.) in time. Making judicious use of the Thomas algorithm, for tridiagonal matrices (see Reference 7), the computed $\dot{T}_j$ were fed into a standard o.d.e. solver contained in the Naval Surface Warface Center Library.[8] The initial conditions are that all $T_j = 0$ except for those on the boundary $\lambda = 0$ where $T = 1$.

NUMERICAL ACCURACY

As stated in the Introduction, an analytical solution is available for the static pore fluid case, $\varepsilon = 0$.[1] Figure 3 compares the analytical (curves) and numerical solutions (symbols) over the range $0 \leqslant \lambda \leqslant 2$ and for dimensionless times 0·1, 0·3, 1·0, 3·0 and 10·0. The largest dimensionless

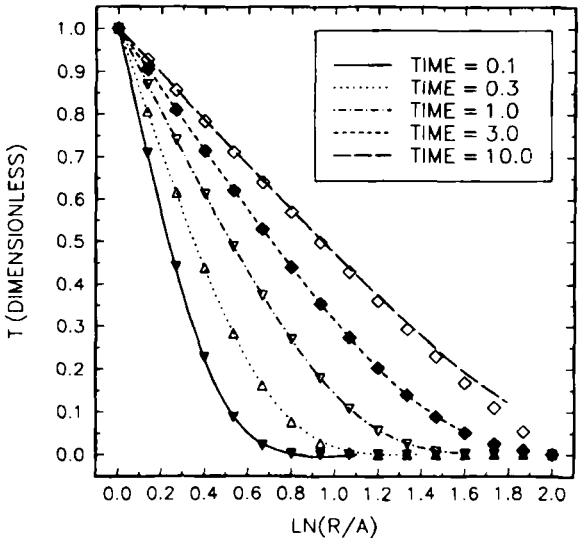

Figure 3. Comparison of numerical results with the known analytical solution for the case $\varepsilon = 0$

time anticipated in typical scenarios would be about 10·0. In all cases, the agreement between the exact and numerical results is very good, with the numerical result typically showing three-digit accuracy. Agreement is best in the immediate vicinity of the cylinder, which is fortunate since the solution gradient near $\lambda = 0$ is required to calculate the power flux emanating from the cylinder surface. As is obvious from Figure 3, accuracy is most likely compromised for large λ and large τ (e.g. inspect the $\tau = 10$ curve for $\lambda \geqslant 1{\cdot}0$). Additional finite element analysis by Arnould[9] in Cartesian space, using a 130-node, 214-element triangular mesh confirmed that numerical accuracy was equally good when $\varepsilon \neq 0$.

NUMERICAL RESULTS

In order to understand the basic features of thermal transport behaviour from heated cylinder to surrounding heterogeneous formation, a parametric study was performed. Those parameters which were subjected to analysis were varied within the ranges given below:

J_0	1×10^{-4} to 10×10^{-4} cm/s
a	4, 8, 16 cm
b	10, 12, 14 cm with $a = 8$ cm
K_a/K_f	0·1–1000
t	1–10 h

All the remaining parameters were held fixed, primarily because there is not likely to be much flexibility in modifying their values. These include:

k_s	0·00462 cal/(s cm °C)
C_{pw}	1·0 cal/(°C cm^3)
$T_a - T_f$	9°C
C_{ps}	0·469 cal/(°C cm^3)
n	0·40

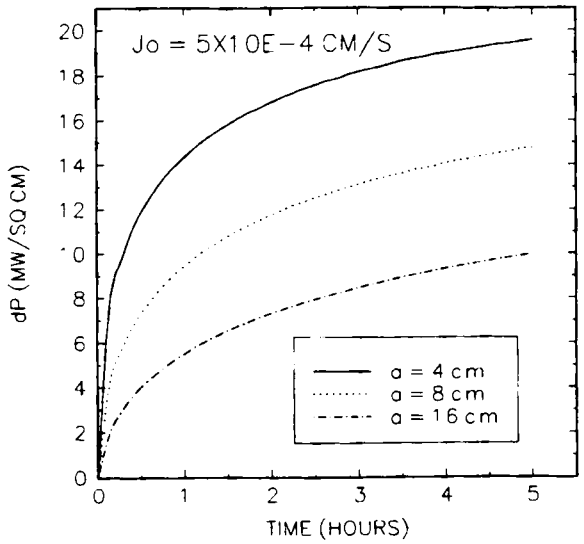

Figure 4. Difference in thermal output between extreme upstream and downstream points on the cylinder surface as a function of time for three different cylinder radii

A simple measure of the extent of asymmetry of thermal output from the cylinder surface to the surrounding medium is the difference in heat flux between the full upstream and full downstream points. Using a water flux of 5×10^{-4} cm/s, this difference in heat flux ($\equiv \delta P$, mw/cm^2) was obtained as a function of time over a 5 h period and for three different cylinder radii. The results, shown in Figure 4, indicate that δp rises quickly in the first hour and has largely levelled off by 5 h. Perhaps the most notable feature of the calculation is the result that a cylinder of smaller radius displays a greater degree of asymmetry. To facilitate a full understanding of this result, we first make a detailed examination of the thermal flux at the cylinder surface, which is proportional to the temperature gradient at $r = a$, $\partial T/\partial r$:

$$\frac{\partial T}{\partial r} = \frac{\partial T}{\partial \lambda}\frac{\mathrm{d}\lambda}{\mathrm{d}r} = \frac{1}{a}\frac{\partial T}{\partial \lambda} \quad (\text{at } r = a) \tag{22}$$

Now the degree of asymmetry should be related to the extent of variation in the temperature gradient itself, along the cylinder perimeter:

$$\delta\left(\frac{\partial T}{\partial r}\right) = \frac{1}{a}\delta\left(\frac{\partial T}{\partial \lambda}\right) \tag{23}$$

However, the variation in the dimensionless gradient can depend only upon the dimensionless parameter ε, which is the only parameter remaining in the governing equation, (13). Indeed, as $\varepsilon \to 0$, the angular variation in temperature gradient will be completely erased. If an analysis were carried out using perturbation methods, the temperature gradient would vary linearly with ε, for very small ε. In the limit of small ε,

$$\delta\left(\frac{\partial T}{\partial r}\right) = \frac{1}{a}\delta\left(\frac{\partial T}{\partial \lambda}\right) \propto \frac{1}{a}\varepsilon = \frac{C_{pw}J_0}{k_s} \tag{24}$$

which clearly shows that an angular variation in thermal output should be essentially independent of 'a' but approximately linearly dependent on the flux J_0. So the question of how radius affects behaviour still remains.

Noting from the dimensionless time relation, equation (14), that radius is squared, we can guess that δP ought to be nearly the same for all cylinder radii, provided that sufficient time has elaspsed. This is readily seen by drawing a horizontal line across Figure 4 at $\delta P = 14$ and observing the times at which this line intersects the $a = 4$ cm and $a = 8$ cm curves. The difference is almost exactly a factor of four. This is precisely what is expected given that real time is scaled by the square of the cylinder radius. A similar result is obtained if another horizontal line is placed at $\delta P = 8$. The intersection times of the two curves, $a = 8$ cm and $a = 16$ cm, again differ by a factor of four. The conclusion then is that thermal output asymmetry is actually independent of radius. Nevertheless, a particular amount of asymmetry occurs at a much earlier time for smaller cylinders. Hence, a velocimeter type instrument based on the measurement of asymmetric thermal output should be smaller rather than larger, if possible.

The analysis leading to equation (24) suggests that the degree of asymmetry in the thermal output ought to be nearly linearly related to J_0, especially if ε is small. A perturbation analysis of equation (13) would undoubtedly lead to such a result. An examination of Figure 5 verifies this expectation. The asymmetry in thermal output, as manifested in δP, shows a near linear growth with J_0 for each of the three cases of probe radius under investigation. Non-linearity would likely be more prevalent as ε is made larger.

The question of how small J_0 may be, and still result in a measurable δP, can now be answered. After 5 h, thermal output from a cylinder of radius 4 cm is 27·5 mw/cm^2, without groundwater flow. With $J_0 = 5{\cdot}0 \times 10^{-5}$ cm/s, the variation in output from full upstream to full downstream, δP, is about 2·2 mw/cm^2. This represents about 8 per cent of the mean output along the cylinder's perimeter. If a measurement of thermal output could only be made with 5 per cent accuracy, then using the heated cylinder as a kind of groundwater velocimeter would be limited to J_0 higher than about $1{\cdot}0 \times 10^{-4}$ cm/s. This result suggests that the preferred design approach would be to devise a measurement scheme that measures δP directly rather than attempt a measurement of thermal output and subsequently calculate δP by difference. A discussion of the prototype device will

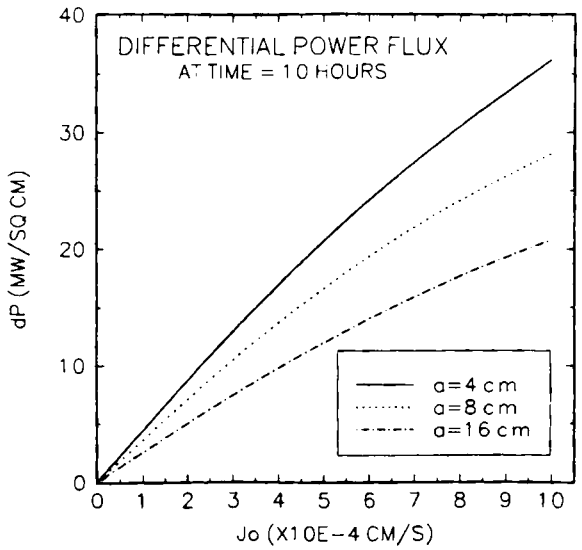

Figure 5. Difference in thermal output between extreme upstream and downstream points on the cylinder surface as a function of groundwater flux. Time = 10 h

describe how δP can be directly measured and thus result in instrument sensitivity greater than $J_0 = 1.0 \times 10^{-4}$ cm/s.

If a heated cylinder is installed into an aquifer for the purpose of velocity measurement, then it becomes important to know the extent to which an annular region, surrounding the cylinder and having different hydraulic properties, might modify the results previously obtained. Some insight into what to expect may be obtained by first calculating an amplification factor, F, which is defined herein as the ratio of water flux in the annular space, with some hydraulic conductivity contrast present ($K_a \neq K_f$), to that in the same region without a contrast in hydraulic conductivity. This factor F is readily computed from equations (3)–(5) and is in fact identical with α:

$$F = \alpha = \frac{2K_a b^2}{b^2(K_a + K_f) - a^2(K_a - K_f)} \tag{5}$$

With $K_a > K_f$, then $F > 1$. As an example, setting $b = 2a$ and $K_a = 10K_f$ yields $F = 2{\cdot}86$. As $b \to a$, this same contrast leads to $F \to 10$. This implies that groundwater is sweeping over the heated cylinder at an increased rate which should enhance asymmetry in thermal output. Figure 6 confirms this logic, though it is perhaps surprising that the δP curves for different values of 'b' are nearly the same. This may be viewed as a consequence of the fact that although F increases as $b \to a$, the thickness of the annular region is dropping, so that the annular region, which supports an increasing water flux, is disappearing. The result that the differential heat flux, δP, is insensitive to the annulus thickness is actually good news for instrument deployment since one need not worry about the precise details of annulus dimensions.

Although controlling the dimensions of an annular region may not be of concern, the effect of varying the hydraulic conductivity of the annular region is still an important issue to consider. Setting $a = 8$ cm and $b = 10$ cm, δP was calculated while the ratio of hydraulic conductivities, K_a/K_f, was varied over four orders of magnitude. The results shown in Figure 7, which pertain to $J_0 = 0{\cdot}0005$ cm/s and $t = 10$ h, form an S-shaped curve when a log scale is used. Fortunately, the

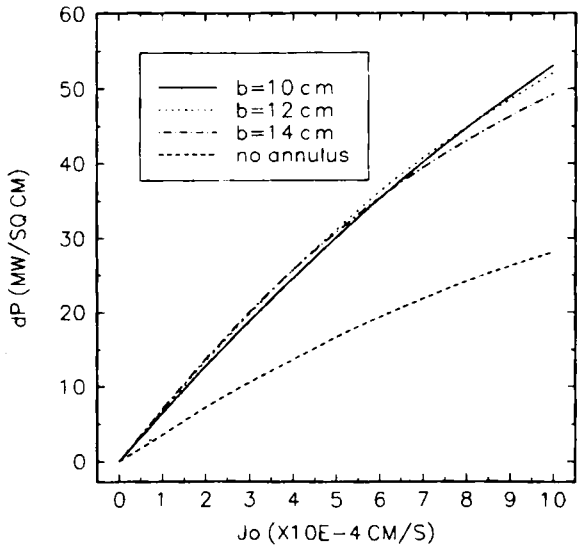

Figure 6. Effect of an annular region, with $K_a = 10 \times K_f$, on the asymmetry in thermal output from the heated cylinder at time = 10 h

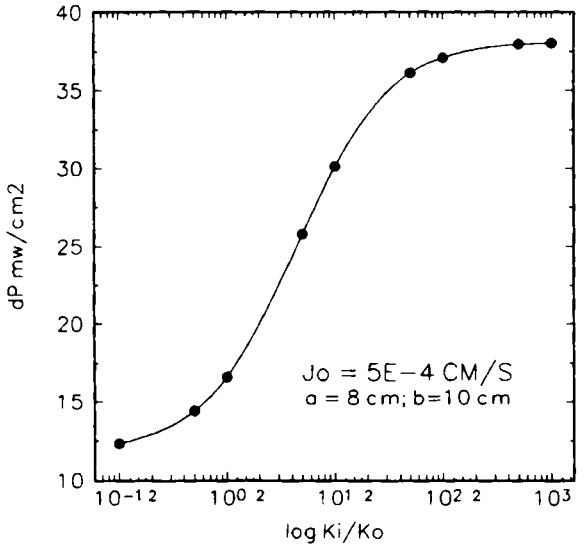

Figure 7. Effect of hydraulic conductivity in the annular region on the asymmetry in thermal output from the heated cylinder. Time = 10 h

point $K_a/K_f = 1$ appears toward the lower left of the S-shape curve so that a reduction in K_a yields little further change in δP. Perhaps in a variety of situations, the installation of a cylindrical object in an aquifer will inadvertently create an annular region having a lower hydraulic conductivity than the formation. As Figure 7 indicates, a 10-fold reduction in K_a results in only a 26 per cent reduction in δP. On the other hand, a 10-fold increase in K_a results in almost a doubling of δP. If the enhanced sensitivity that comes from a large K_a/K_f is to be used with advantage, then K_a should be at least two orders of magnitude larger than K_f. Then, the precise values of K_a and K_f need not be known. In fact, the sensitivity of a 'heated-cylinder velocimeter' becomes independent of K_a and K_f, as is shown in Figure 7 and by the limiting value for the parameter F:

$$F \rightarrow \frac{2b^2}{b^2 - a^2}$$

which is, of course, dependent only on geometry. In this case, $F = 2{\cdot}67$ when $b = 2a$. Note that both α and β approach limiting values that depend only on 'a' and 'b'.

A PROTOTYPE VELOCIMETER

The results of calculations strongly suggest that it is worthwhile attempting to construct and test a 'heated-cylinder velocimeter' (hereafter, simply referred to as probe). Thus, a device was built and some preliminary results will be discussed. First, a brief discussion of the manner of probe construction will be given.

With reference to Figure 8, the probe consists primarily of two concentric cylinders, an inner one prepared from high strength nylon 6 (5·25 inch outer diameter), and an outer one from ordinary PVC water pipe (6·0 inch internal diameter and 0·25 inch wall thickness). The inner cylinder of length 12·0 inch was threaded to accept about 175 ft of # 18 nichrome wire to serve as a primary heating element. The resistance of the primary heating element is about 78 Ω. Fourteen

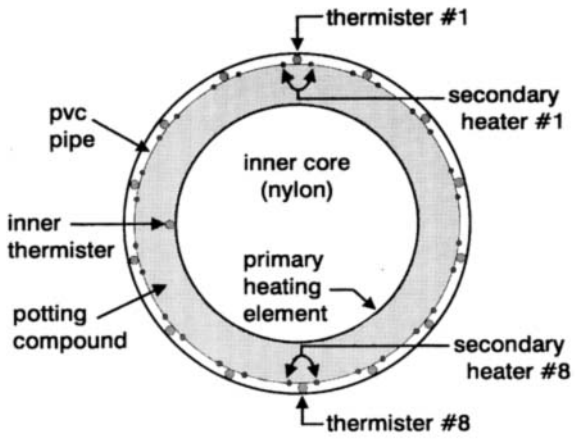

Figure 8. Sketch of prototype heated-cylinder groundwater 'velocimeter'

thermistors* were installed along the perimeter of the outer cylinder, in equally spaced holes in the cylinder's wall (only two are specifically labelled). This ring of thermistors is located 7·0 inch from either end of the 14·0 inch long outer cylinder. A 15th thermistor was affixed to the primary heater winding as depicted in Figure 8. Their resistance at 25·0°C is 3000 Ω and they were sealed into their respective holes using an epoxy glue. Additional insulated hook-up wire was soldered to the thermistors and led out through the end of the cylinder along its wall.

A secondary heating element was installed at each of the thermistor locations on the inner wall of the outer PVC cylinder. These 14 heaters were prepared from # 32 nichrome wire and attached as follows. A pair of binding posts (like those used on wire-wrap circuit boards) was mounted near the end of the PVC cylinder, spaced about 0·25 inch apart. One end of the secondary heating wire was wrapped around a binding post just prior to press fitting the binding post into a small hole in the PVC pipe. The wire was then run along the length of the cylinder to its other end where it was passed through a pair of small holes (again 0·25 inch apart) and then returned to the other side where it was attached to the second binding post in the same manner as the first. In this way, the secondary heating elements straddle their companion thermistors and the two leads from these heating elements are both conveniently led out of the same end of the probe. With careful construction, these heaters had resistances of 22·3 $\pm$ 0·1 Ω. All holes passing through the PVC pipe were filled with epoxy glue.

The smaller cylinder with its primary heater was placed co-axially inside the larger PVC pipe and centred with the aid of Plexiglas spacers (0·25 inch diameter rod) on one end and a circular nylon 6 plate on the other. The annular gap was filled with a silicone rubber potting compound, RTV627A.† Its unhardened consistency is like that of latex paint. When hardened, its tensile strength is 500 psi.

The bulk of the heat discharged to the surroundings is supplied by the internal primary heater, and the secondary heaters should not be needed at all in the event that the groundwater is static. This follows since, then, isothermal conditions will naturally prevail on the probe surface. Only when groundwater is moving will there be a tendency for upstream points on the probe surface to

*Yellow Springs Instrument Company, Inc., Yellow Springs, OH 45387

†G. E. Co., Silicone Products Div., RTV Products Dept., Waterford, NY 12188

run cooler, as monitored by thermistors. Hence, the function of the outer ring of thermistors and their companion secondary heaters is to maintain as nearly as possible the same temperature along the entire perimeter of the PVC pipe. Of course, those secondary heaters that are located farther upstream are expected to discharge more heat into the surrounding soil in order to fulfil the spatially isothermal requirement under non-static conditions. In fact, measuring the heat discharged via the secondary heaters is equivalent to the direct measurement of δP, already discussed, multiplied by the surface area allocated to a particular secondary heater.

The electronics needed to achieve the goals stated in the previous paragraph are quite involved and will not be discussed here. These details are reserved for a future paper that will focus specifically on the experimental method. For now, it is simply noted that the support electronics, together with thermistors and secondary heaters, held the angular variation in probe surface temperature beneath 0·2°C. The inner thermistor shown in Figure 8 was involved in 'compensation' circuitry that corrected for certain unavoidable instrument imperfections. Again, these are details for a later publication.

EXPERIMENTAL RESULTS

The prototype was tested in a laboratory sandbox approximately 1·5 m^2 and 0·5 m deep. The box was filled with a medium sand that had a packed porosity of about 0·4. The measured thermal properties for this sand were given previously. They are nearly identical to that given by Molson *et al.*[10] A metering pump was used to force the flow of water through the sand at the desired flow rate. Though it is perhaps feasible to use the laboratory measured response of the probe as a function of discharge velocity for calibration purposes, the intent here is to use the previously described model to interpret the observed probe response so as to yield the flux, J_0.

Figure 9 examines the reproducibility of probe response in two different 10 h experiments, one at $J_0 = 2{\cdot}43 \times 10^{-4}$ cm/s and the other at $J_0 = 2{\cdot}33 \times 10^{-4}$ cm/s. A target temperature of 31°C

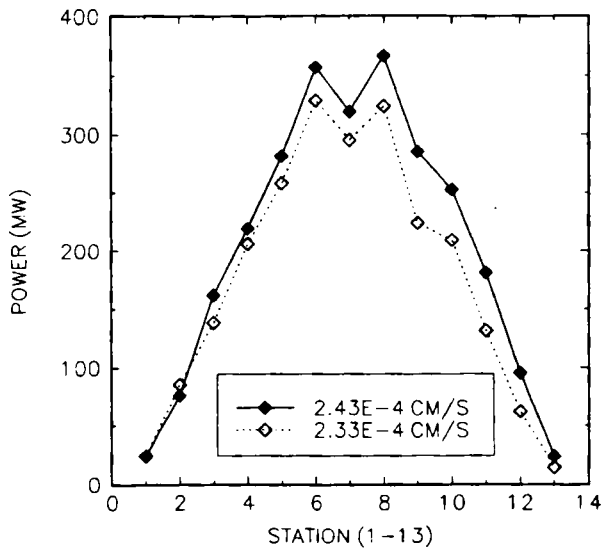

Figure 9. Power output from secondary heaters as a function of location on the surface of the heated cylinder. Secondary heater #14 is at the full downstream position and left unheated. Results are for two similar values of J_0 to check reproducibility

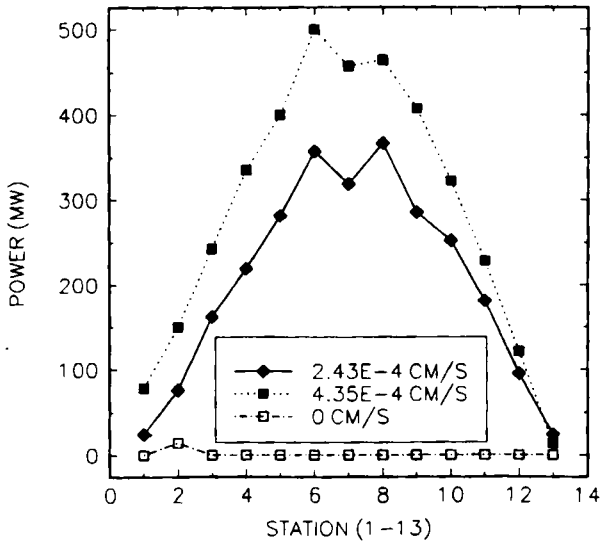

Figure 10. Power output from secondary heaters as a function of location on the surface of the heated cylinder. Results are shown for three different values of J_0

was achieved in about 30 min in a sand tank that started out at 22°C. The ordinate in the figure gives the electrical power, dissipated as heat into a particular secondary heater, while the abscissa identifies a particular secondary heater or 'station'. As the figure indicates, power output varies smoothly from one station to the next, exhibiting larger values for those secondary heaters located farther upstream. The secondary heater at the full downstream position was left unpowered. Reproducibility is quite good given that the two curves nearly overlie one another.

Figure 10 shows the effect on probe response of varying the discharge flux through the sand tank. Results for three different fluxes are shown, varying from 0·0 to 4.35×10^{-4} cm/s. With no flow, the secondary heaters produce negligible output as depicted in the figure. The upper curve pertains to the higher flow and should give a response nearly 1·8 times greater than the middle curve, which corresponds to a flux of $2{\cdot}43 \times 10^{-4}$ cm/s. This is expected since Figure 5 indicates a near linear relationship between δP and J_0 in the flow range under examination. The data indicate, however, that the upper curve reflects an increase over the middle curve by a factor of 1·4. The origin of the discrepancy is not yet known. Another feature of the experimental data that is as yet inexplicable is the dip in power output at station 7, the extreme upstream point on the probe. Ideally, power output would smoothly rise to a maximum as station 7 is approached. Given that more heat is discharged into surrounding sand at this particular point, it is possible that the mild heating of pore water forces some small amount of dissolved gas out of solution so that a thermally insulating layer or zone of trapped gas bubbles forms at the full upstream point. This is, however, just speculation.

Using the model previously discussed, an attempt was made to simulate the responses observed in Figures 9 and 10. In order to do this, a value for thermal conductivity was needed to complete the set of parameters required by the model. Heater power is known at any time during an experiment for all heaters and thus provides for an easy way to measure the total thermal output. For a no flow experiment with target temperature set to 9°C above ambient, the power output was approximately 24 w after 10 h. Thermal conductivity was varied in an iterative manner until the analytical solution of Jaeger[1] gave a power output in reasonable agreement with this value.

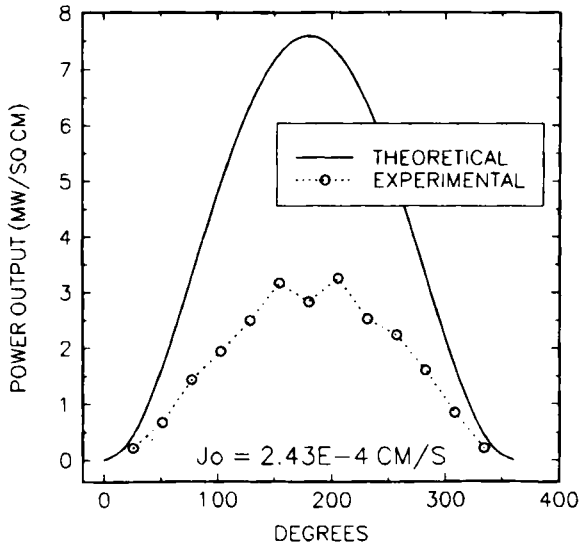

Figure 11. Comparison of theoretical results with experimental for a single value of J_0. Experimental results are now expressed as power output per unit area to facilitate comparison with theory

The value for thermal conductivity obtained through this inverse solution procedure was 0·00462 cal/(s cm °C). To put this number in perspective, Bear[6] gives values of 0·009 for sandstone, 0·005 for limestone, 0·004–0·01 for dolomite and 0·002–0·003 for clay. Certainly, the correct value should lie in the range 0·0011 for water to 0·02 for quartz. The harmonic mean of these two values, weighted according to their respective volume fractions, was 0·00254 whereas the arithmetic mean, again weighted by volume fractions, was 0·0124.The porosity of the sand was approximately 0·4. Obviously, the harmonic mean gives somewhat better agreement with the number obtained here.

Figure 11 compares the experimental results, obtained with a discharge flux of $2{\cdot}43 \times 10^{-4}$ cm/s after 10 h, with theoretical results. The target temperature was 9·0°C above ambient. Clearly, the theoretical results overpredict the observed response by about a factor of 2·5. Nevertheless, a factor of 2·5 still represents a sizeable improvement over modern field techniques which provide velocities that are only order-of-magnitude accurate. At this point, only speculation over the source of the discrepancy can be offered. The extent to which any of the assumptions in the model are unrealistic is unknown. Since the Peclet number is much smaller than one, it still seems reasonable to say that mechanical dispersion is unimportant. Whether or not a natural convection event occurred is unknown, but since efforts were made to deliberately exclude vertical temperature gradients, it seems reasonable to ignore natural convection. Heat transport is expected to be essentially horizontal within a sand layer having a depth that equals the probe length.

The simulations assumed that the probe surface temperature reached the intended target temperature immediately, which was not the case. Rather, the intended target temperature was only reached in about $\frac{1}{2}$ h. This would undoubtedly cause the experimental result to be less than theoretical, given the results of Figure 4, but could not account for a major portion of the discrepancy. Other aspects of these initial experiments, which might account for the observed behaviour of the prototype, are currently under evaluation. Nevertheless, initial theoretical and experimental results are sufficiently encouraging that a velocimeter of smaller radius is currently undergoing design and construction.

ACKNOWLEDGEMENT

This work was partially supported by a grant from the National Science Foundation.

REFERENCES

1. J. C. Jaeger, 'Numerical values for the temperature in radial heat flow', *J. Math. Phys.* **34**, 316–321 (1956).
2. J. G. Melville, F. J. Molz and O. Güven, 'Laboratory investigation and analysis of a ground-water flowmeter', *Ground Water*, **23**, 486–495 (1985).
3. J. C. Dunn, H. C. Hardee and R. P. Striker, 'Convective heat flow probe', *U. S. Patent Number 4547080*, 1985.
4. C. A. van der Star, G. A. M. van Meurs and C. J. Hoogendoorn, 'Heat exchange between a tube and water-saturated soil', *J. Solar Energy Eng.*, **108**, 298–302 (1986).
5. J. R. Reitz and F. J. Milford, *Foundations of Electromagnetic Theory*, 2nd edn, Addison-Wesley, Reading, MA, 1967, pp. 52–53.
6. J. Bear, *Dynamics of Fluids in Porous Media*, American Elsevier, New York, NY, 1972.
7. L. Lapidus and G. F. Pinder, *Numerical Solution of Partial Differential Equations Science and Engineering*, Wiley, New York, NY, 1982, p. 216.
8. A. H. Morris, Naval Surface Warfare Center Library of Mathematics Subroutines, Naval Surface Warfare Center, Dahlgren, VA, January 1993.
9. R. Arnould, 'Finite element modeling of thermal output from a heated probe in flowing groundwater', *M. S. Thesis*, Northwestern University, 1992.
10. J. W. Molson, E. O. Frind and C. D. Palmer, 'Thermal energy storage in an unconfined aquifer 2. Model development, validation, and application, *Water Resources Res.*, **28**, 2857–2867 (1992).